ELSEVIER

Chemical Engineering Journal 128 (2007) 21–32

Chemical Engineering Journal

www.elsevier.com/locate/cej

Oxygen transfer from growing bubbles: Effect of the physical properties of the liquid

Mariano Martín *, Francisco J. Montes, Miguel A. Galán

Departamento de Ingeniería Química y Textil, Universidad de Salamanca, Pza. de los Caídos 1-5, 37008 Salamanca, Spain

Received 24 March 2006; received in revised form 22 August 2006; accepted 3 October 2006

Abstract

Mass transfer from bubbles generated at dispersion devices is a major operation in chemical engineering. Most mass transfer models have focused on the free rising of the bubbles, but the bubbling process plays an important role because it determines the bubbles' initial volume, surface area and oscillation amplitude. In this work, the mass transfer mechanism and the shape of a single growing bubble are studied by combining a hydrodynamic model and a mass transfer model, given by Higbie's theory. The complete model has been tested using both, Newtonian and non-Newtonian fluids. Calculated bubble shapes, areas, volumes and detachment times are compared with those recorded by a high speed video camera device in a deoxygenated media. Good agreement is achieved between the results of the models and the experimental recordings. Furthermore, the effect of the physical properties of the liquid, viscosity, density and surface tension, on the Sherwood number of a growing bubble has been studied using the theoretical model. The liquid viscosity and the surface tension increase the Sherwood number meanwhile the liquid density reduces it. A dimensionless expression for the Sherwood number in terms of the Reynolds and the Schmidt numbers has also been developed.

Keywords: Bubble model; Detachment time; Sieve plates; Mass transfer; Sherwood

1. Introduction

Gas–liquid processes, where a gas phase is dispersed into a liquid phase to provide the reactants required for the chemical or the biochemical reaction, are very common in order to treat water wastes or heavy metals and for producing several chemical and biochemical compounds. These processes depend largely on the mass transfer rate from the bubbles generated at dispersion devices, which, most of the times, is the limiting factor [1–6].

Bioprocesses involving cell cultures can be sensitive to high hydrodynamic stresses leading to an important decrease in cellular viability. Bubble columns and sieve plate towers are the most adequate aeration devices for these types of cultures [7,8]. These devices generate dispersions of a gas phase in a liquid phase or in a slurry, in order to improve the contact between the phases, increasing the available surface for mass transfer [1–4,6,9].

Numerous studies regarding mass transfer in bubble columns provide empirical correlations for the volumetric mass transfer coefficient, k_La [1,4,9]. The penetration theory, proposed by Higbie [10], exposed a mass transfer mechanism responsible for the property transport which has become the base for most of the empirical correlations used to predict k_La.

The study of the mechanism of mass transfer from an individual bubble attempts to improve the understanding and to give an insight of the process, so that the design of the equipment can be optimized.

Several papers have studied the mass transfer rate from individual rising bubbles, not only for spherical bubbles [11–13], but also for ellipsoids or spherical cup bubbles [14], as well as for oscillating ones [15], by means of studying the hydrodynamics surrounding the bubble. Several expressions for the Sherwood number have been developed.

However, the mass transfer rate during the formation of the bubbles has been barely studied, either by measuring the bubble surface area photographically and using the Higbie's theory [16], or by modelling a particular case of bubble formation including mass transfer from the bubbles [17]. The model was based on a previous hydrodynamic model [18], using the Higbie's theory to simulate the mass transfer rate under unsteady conditions. This process included diffusional mass transfer and chemical absorption of ammonia in water. Despite the fact that the enhancement factor was taken to be 1 and the model detachment time was

* Corresponding author. Tel.: +34 923294479; fax: +34 923294574.
E-mail address: mariano.m3@usal.es (M. Martín).

1385-8947/$ – see front matter © 2006 Elsevier B.V. All rights reserved.
doi:10.1016/j.cej.2006.10.004

Nomenclature

a	bubble superficial area (m^2)
A_t	orifice cross sectional area (m^2)
A_1	gas chamber cross sectional area (m^2)
C	added mass coefficient
C_s	loss coefficient
C_D	drag coefficient
C^*	saturation concentration ($kg\,m^{-3}$)
D_o	orifice diameter (m)
D_G	gas diffusivity ($m^2\,s^{-1}$)
D_L	liquid diffusivity ($m^2\,s^{-1}$)
fc	retention factor
g	gravity ($m\,s^{-2}$)
Gr	Grashof number, $Gr = d_{eq}^3 \rho \Delta\rho g/\mu^2$
H	Henry constant ($mol\,Pa^{-1}\,m^{-3}$)
H_L	liquid height (m)
j	superficial element
k_L	liquid side resistance ($m\,s^{-1}$)
k_La	liquid side mass transfer coefficient (s^{-1})
K_La	global mass transfer coefficient (s^{-1})
l^*	contact interface length (m)
m	gas mass in bubble (kg)
m_f	power law coefficient ($Pa\,s^{n^*}$)
M	virtual mass (kg)
n	final bubble point
n^*	power law exponent
P_{atm}	atmospheric pressure (Pa)
P_B	bubble pressure (Pa)
P_C	chamber pressure (Pa)
P_H	hydrostatic pressure (Pa)
P_M^{air}	average molecular weight of air ($kg\,mol^{-1}$)
Q_B	bubble gas flow rate ($m^3\,s^{-1}$)
Q_C	chamber gas flow rate ($m^3\,s^{-1}$)
r	radial coordinate (m)
r'	z derivative of radial coordinate
R	bubble radius (m)
R_g	gas constant ($J\,mol^{-1}\,K^{-1}$)
Re	Reynolds number, $Re = \rho u_0 d_{eq}/\mu$
Re_B	Reynolds number of the bubble: Newtonian fluids, $Re_B = \rho U_z D_{max}/\mu$; non-Newtonian fluids, $Re_B = \rho U_z^{2-n^*} D_{max}/m_f$
RG	gas phase resistance ($s\,m^{-1}$)
RI	gas–liquid interface resistance ($s\,m^{-1}$)
RL	liquid phase resistance ($s\,m^{-1}$)
Sc	Schmidt number, $Sc = \mu/\rho D_L$
Sh	Sherwood number, $Sh = k_L d_{eq}/D_L$
t	growing time (s)
T	temperature (K)
u_o	orifice gas velocity ($m\,s^{-1}$)
U_r	horizontal velocity ($m\,s^{-1}$)
U_z	rising velocity ($m\,s^{-1}$)
V_B	bubble volume (m^3)
V_C	gas chamber volume (m^3)
z	j point real height (m)
z'	j point apparent height (m)

Greek letters

α	evaporation
α_L	liquid fraction in the column
θ	angle between the axis of symmetry of the bubble and the radius of curvature at any point (rad)
μ_L	liquid vicosity (Pa s)
μ_G	gas viscosity (Pa s)
ρ_G	gas density ($kg\,m^{-3}$)
ρ_L	liquid density ($kg\,m^{-3}$)
σ	superficial tension ($N\,m^{-1}$)

Subscript

liq	liquid phase

lower than the experimental one, the model produced good results.

The mass transfer process in bubble columns depends strongly on the rising stage of the bubbles, which is characterised by the rising path and the oscillatory behaviour of the bubbles. Both are determined by the size of the grown bubbles at the detachment point [3,15]. Furthermore, the mass transfer rate of the growing bubble corresponds to the initial condition for the mass transfer during the rising of the bubbles.

The wide range of processes carried out in a bubble column, such as oxidation, chlorination, alkylation, polymerization and hydrogenation, in the manufacture of synthetic fuels by gas conversion processes and in biochemical processes such as fermentation and biological wastewater treatment [4], broaden the characteristics of the liquid phases inside the equipment, inviscid, viscous, slurries, etc. Moreover, during many of those processes, wastewater treatment, fermentations, etc., the physical properties of the liquid change with time [19–21]. The physical properties of the liquid surrounding the bubbles not only determine the bubble formation [22], with its effect on the bubble initial size, but also determine transport properties like the liquid diffusivity [23].

Therefore, the present paper deals with the mass transfer mechanism from single air bubbles generated at a sieve plate of a bubble column. The liquid media were Newtonian and non-Newtonian power law fluids (water and a 1.4% CMC solution in water), which are typical rheological behaviours [9]. The liquids, which were deoxygenated to allow the oxygen transfer from the bubbles to the liquid bulk, can be considered as stagnant, due to the low gas flow rates used ($(1–10) \times 10^{-6}\,m^3\,s^{-1}$) to avoid vertical coalescence of the growing bubbles and the dimensions of the experimental bubble column ($15\,cm \times 15\,cm \times 20\,cm$), made of flat glass walls to avoid distortions in the recordings. The experimental recordings of the bubble formation process with mass transfer are compared with a modified hydrodynamic model [22,24] to verify it.

The effect of the physical properties of the liquid on the mass transfer rate has been theoretically studied by means of the proved model, and summarised in the Sherwood number for a growing bubble, which was correlated versus the same dimensionless numbers as those proposed by several authors [25–27].

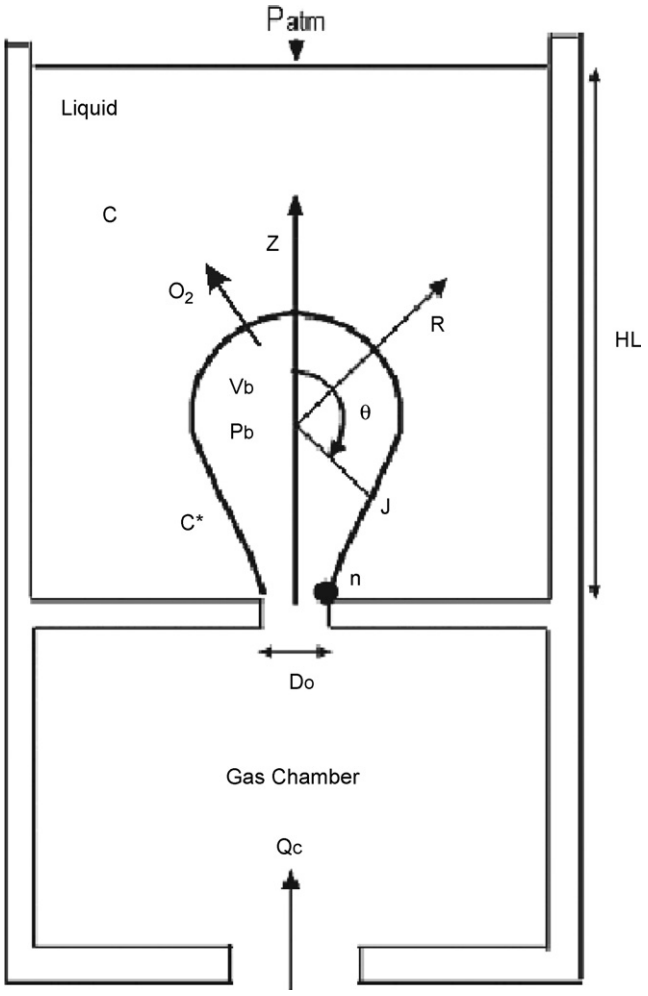

Fig. 1. Schematic representation of the generation of a gas bubble in a submerged orifice.

2. Theoretical considerations

Axisymmetric bubble models for Newtonian and non-Newtonian fluids [22,24] are the base for the present model. A schematic representation of the system is shown in Fig. 1. The bubble is discretized into 100 points from the top to the bottom of the figure.

2.1. The hydrodynamic model

The hydrodynamic model consists of two different stages. The first stage corresponds to the generation of a gas bubble in a stagnant liquid while it is attached to the perimeter of the orifice. It is considered that in the experimental bubble column, next to the sieve plate, there are no fluid flows due to the working conditions, see equipment. The second corresponds to the rising of the bubbles before the onset of the oscillations. Both stages are modelled by means of a momentum balance, and a force balance.

The momentum balance determines the bubble expansion, taking into account the surface tension, responsible for the stability of the shape of the bubble, and the viscosity of the liquid, a resistance for the expansion of the bubble. In spherical coordinates a momentum balance can be written as

$$\frac{\partial u_r}{\partial t} + u_r \frac{\partial u_r}{\partial r} = -\frac{1}{\rho_L}\frac{\partial p}{\partial r} - \frac{1}{\rho_L}[\text{div}\,\tau]_r \tag{1}$$

where

$$u_r(r,t) = \frac{R^2(\mathrm{d}R/\mathrm{d}t)}{r^2} \tag{2}$$

Substituting Eq. (2) into Eq. (1) and integrating Eq. (1) from the surface of the bubble to infinity, it yields:

$$R\frac{\mathrm{d}^2R}{\mathrm{d}t^2} + \frac{3}{2}\left(\frac{\mathrm{d}R}{\mathrm{d}t}\right)^2 = \frac{P_L - P_\infty}{\rho_L} - \frac{1}{\rho_L}\int_R^\infty [\text{div}\,\tau]_r\,\mathrm{d}r \tag{3}$$

The divergence of the shear stress can be described in terms of its three normal components. As the liquid is considered to be incompressible, the only active component of the stress will be the radial component. Besides, the pressure at infinite is equal to the hydrostatic pressure. Under these considerations, Eq. (3) becomes:

$$R\frac{\mathrm{d}^2R}{\mathrm{d}t^2} + \frac{3}{2}\left(\frac{\mathrm{d}R}{\mathrm{d}t}\right)^2 = \frac{P_L - P_H}{\rho_L} + \frac{\tau_{rr}|_{r=R}}{\rho_L} - \frac{3}{\rho_L}\int_R^\infty \frac{\tau_{rr}}{r}\,\mathrm{d}r \tag{4}$$

where

$$P_L + \tau_{rr}|_{r=R} + \frac{2\sigma}{R} = P_B \tag{5}$$

P_B is the gas pressure inside the bubble, and

$$P_H = P_{atm} + \rho_L g(H_L - z) \tag{6}$$

The integral of the shear stress depends on the rheological behaviour of the liquid, lets it be P_μ

$$P_\mu = 3\int_R^\infty \frac{\tau_{rr}}{r}\,\mathrm{d}r \tag{7}$$

Thus Eq. (4) can be rewritten as follows:

$$\rho_L\left(R\frac{\mathrm{d}^2R}{\mathrm{d}t^2} + \frac{3}{2}\left(\frac{\mathrm{d}R}{\mathrm{d}t}\right)^2\right) = P_B - P_H - \frac{2\sigma}{R} - P_\mu \tag{8}$$

For a Newtonian fluid, the shear stress tensor can be expressed as

$$\tau_{rr} = -2\mu_L\frac{\partial u_r}{\partial r} = 4\mu_L\frac{R^2(\mathrm{d}R/\mathrm{d}t)}{r^3} \tag{9}$$

So P_μ becomes:

$$P_\mu = \frac{4\mu_L}{R}\frac{\partial R}{\mathrm{d}t} \tag{10}$$

In case of working with a Newtonian liquid Eq. (8) can be rewritten as follows:

$$P_B - P_H = \rho_L\left[R\frac{\mathrm{d}^2R}{\mathrm{d}t^2} + \frac{3}{2}\left(\frac{\mathrm{d}R}{\mathrm{d}t}\right)^2\right] + \frac{2\sigma}{R} + \frac{4\mu_L}{R}\frac{\mathrm{d}R}{\mathrm{d}t} \tag{11}$$

If the working liquid behaves as a non-Newtonian power law liquid, instead of using Eq. (10) Li et al. [28], proposed Eq. (12).

$$P_\mu = \frac{4m_f(2\sqrt{3})^{n*-1}}{n^*}\left(\frac{dR/dt}{R}\right)^{n*} \quad (12)$$

The second balance, the force balance, determines the rising of the bubble. It considers the buoyancy of the bubble, the drag forces, the inertial forces due to the gas flow rate across the orifice along with those due to the liquid dragged by the bubble as it rises, and the gas–liquid–plate interactions [24].

$$\frac{d}{dt}\left(M'\frac{dz'}{dt}\right) = (\rho_L - \rho_G)V_B g fc - \frac{1}{2}C_D\rho_L\left(\frac{dz'}{dt}\right)^2\frac{\pi {D_{max}}^2}{4} + \frac{4\rho_G}{\pi D_o^2}\left(\frac{dV_B}{dt}\right)^2 \quad (13)$$

The added mass is defined as Eq. (14).

$$M' = (\rho_G + C\rho_L)V_B \quad (14)$$

where the added mass coefficient, C, is taken to be 11/16 and fc = 0.005, during the growing stage of the bubble [22].

The drag coefficient depends on the rheological behaviour of the liquid. When the liquid behaves as a Newtonian one, the drag coefficient can be calculated using the equations proposed by Loubière and Hébrard [29]:

$$C_D = \frac{24}{Re_B}(1 + 0.15Re_B^{0.687})\alpha_L^{-1.7}, \quad Re_B < 1000 \quad (15)$$

$$C_D = 0.44, \quad Re_B > 1000 \quad (16)$$

In the experimental conditions used, $\alpha_L \simeq 1$. The gas phase in the bubble column is negligible compared to the liquid phase to avoid interferences among bubbles.

In case of working with non-Newtonian power law liquids, the equations proposed by Kelesidis [30], are used to calculate C_D:

$$C_D = [2.25{Re_B}^{-0.31} + 0.36{Re_B}^{0.06}]^{3.45} \quad (17)$$

The Reynolds number for the bubble is defined as

$$\text{Newtonian liquid, } Re_B = \frac{\rho U_z D_{max}}{\mu};$$

$$\text{non-Newtonian power law liquid, } Re_B = \frac{\rho_L D_{max}(U_z)^{2-n^*}}{m_f} \quad (18)$$

where U_z is the vertical velocity. The drag coefficient is applied for the points with a z coordinate higher than that which corresponds to the maximum diameter.

The radial velocity, U_r, of the points of the bubble surface depends on the expansion of the bubble. The spherical coordinates must be transformed into Cartesians.

$$U_r = \frac{dr}{dt} = \frac{dR}{dt}\sin(\theta) \quad (19)$$

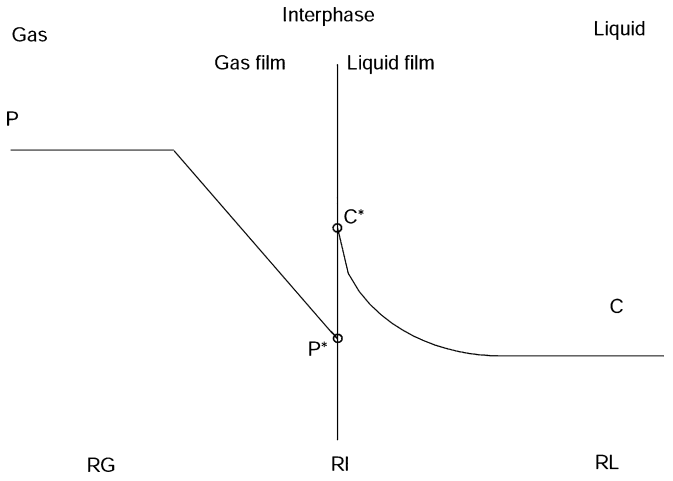

Fig. 2. Mass transfer through bubble surface.

The vertical velocity, U_z, is calculated as a composition between the rising movement, given by the force balance, and the expansion, determined by the momentum balance. The presence of the plate avoids an expansion of the bubble against it during the growing so, an upward force is developed for the points located under the maximum diameter of the bubble [24].

$$U_z = \frac{dz}{dt} = \frac{dz'}{dt} + \text{abs}\left(\frac{dR}{dt}\cos\theta\right) \quad (20)$$

The detachment of the bubble from the sieve plate occurs when the thickness of the bubble neck is smaller than 1 μm. The system reaches a state of minimum of energy related to the quasi-spherical shape of the bubble [24]. Once the bubble has detached, inertial forces due to the orifice and the terms related to the presence of the plate are modified so, $C = 0.5$ and fc = 1 [24], and Eq. (13) becomes Eq. (21):

$$\frac{d}{dt}\left(M'\frac{dz'}{dt}\right) = (\rho_L - \rho_G)V_B g - \frac{1}{2}C_D\rho_L\left(\frac{dz'}{dt}\right)^2\frac{\pi D_{max}^2}{4} \quad (21)$$

And the rising velocity for all the points will be:

$$U_z = \frac{dz}{dt} = \frac{dz'}{dt} + \frac{dR}{Et}\cos\theta \quad (22)$$

2.2. Mass transfer mechanism

The concentration gradient is expressed as: $\Delta C_{O_2} = C^* - C_{liq}$.

The mass transfer mechanism in a two-phased system includes three resistances placed in series (Fig. 2). Those resistances correspond to the resistances due to the liquid bulk, the gas bulk and the interface.

Higbie proposed the penetration theory for unsteady mass transfer at the gas–liquid interface [10], such as bubble growth and an accelerating rising bubble [17]. Higbie's penetration theory proposes a liquid resistance k_L at gas–liquid contacting time

t given by Eq. (23) [10,17]:

$$k_L = \sqrt{\frac{4D_L}{\pi t}} \tag{23}$$

D_L is the liquid diffusivity. The interfacial resistance is calculated using Eq. (24) [31]:

$$k_I = \frac{1006\alpha}{\sqrt{2\pi R_g T}} \tag{24}$$

where α is 1 for most of the liquids, including water [13].

The gas phase resistance, due to the convective mass transfer of the gaseous solute from the bulk of the gas, can be determined following Eq. (25) [31], with $D_G = 1 \times 10^{-5}$ m^2 s^{-1}, $\mu_G = 1.7 \times 10^{-5}$ kg/m s [3]:

$$\frac{k_G l^*}{D_G} = 0.664\left(\frac{\rho_G u_o l^*}{\mu_G}\right)^{1/2}\left(\frac{\mu_G}{\rho_G D_G}\right)^{1/3} \tag{25}$$

where l^* is the length of the contact surface and is calculated measuring the bubble contour at each time step.

The global mass transfer coefficient is calculated considering all the described resistances:

$$\frac{1}{K_L} = \frac{H}{k_G} + \frac{H}{k_I} + \frac{1}{k_L} = \mathrm{RG} + \mathrm{RI} + \mathrm{RL} \tag{26}$$

Henry's constant for air water at 20 °C is (1/73,200) mol/m^3 Pa [32].

2.3. Coupling mass and momentum transfers

To calculate the pressure inside the bubble, P_B, for the momentum balance, Eq. (8), a mass balance to the gas chamber–bubble system will be developed. The mass balance of the hydrodynamic model [22,24], must be modified to take into consideration the oxygen transfer from the bubble to the liquid bulk.

The internal pressure of the gas in the bubble depends on the mass inside the bubble. Considering an ideal behaviour of the air:

$$P_B = m(t)\frac{R_g T}{P_M^{air} V_B} \tag{27}$$

To calculate the mass which has entered the bubble, it is considered the pressure loss across the orifice:

$$\frac{dm}{dt} = \frac{C_s A_t}{\sqrt{1-(A_t/A_1)}} 2\rho_G \sqrt{P_B - P_C} - K_L a \Delta C_{O_2} \tag{28}$$

C_s is 0.6 for perforated plates [33].

A mass balance to the gas chamber–bubble system, considering polytropic behaviour of the gas in the chamber, provides the pressure in the gas chamber, P_C:

$$\frac{dP_C}{dt} = \frac{\kappa P_C}{V_C}(Q_C - Q_B) = \frac{\kappa P_C}{V_C}\left(Q_C - \frac{dV_B}{dt} - \frac{K_L a \Delta C_{O_2}}{\rho_G}\right) \tag{29}$$

The polytropic coefficient of the air is $\kappa = 1.4$.

The volumetric flow rate entering the bubble is related to the rate of mass entering the bubble by

$$\frac{dV_B}{dt} = \frac{dm}{dt}\frac{1}{\rho_G} \tag{30}$$

The gas density is recalculated internally during the integration procedure:

$$\rho_G = \frac{P_B P_M^{air}}{R_g T} \tag{31}$$

Once the bubble has detached, when the resulting neck is close enough to the z-axis, the interface surrounding the neck collapses. The bubble volume is determined graphically by means of a revolution integral [34], from the n point (bottom of Fig. 1), to point 1 (top of the Fig. 1). Gas density is recalculated every time step using the remaining mass inside the bubble and the bubble volume calculated graphically using Eq. (32).

$$V_B = \sum_{j=1}^{j=N-1} \pi \int_{z_j}^{z_{j+1}} (r(z))^2 \, dz \tag{32}$$

where

$$r(z) = \left(\frac{r_{j+1} - r_j}{z_{j+1} - z_j}\right)(z - z_j) + r_j \tag{33}$$

The initial mass inside the bubble is calculated from the mass inside the volume before the detachment. Afterwards, the bubble will only lose mass due to the transfer to the surrounding liquid according to Eq. (34):

$$\frac{dm}{dt} = -K_L a \Delta C_{O_2} \tag{34}$$

2.4. Superficial area

Mass transfer is strongly affected by the available contact area. In this work, the available area is calculated as the surface generated by a revolution body around the z-axis [34]:

$$a = \sum_{j=1}^{j=N-1}\left(2\pi \int_{z_j}^{z_{j+1}} r\sqrt{1 + (r')^2}\, dz\right) \tag{35}$$

where the r coordinate as function of z can be expressed as

$$r(z) = \left(\frac{r_{j+1} - r_j}{z_{j+1} - z_j}\right)(z - z_j) + r_j \tag{36}$$

2.5. Initial and boundary conditions for the numerical solution

Apart from the initial conditions (m ($t = 0$) is equal to the mass of a semi spherical bubble of radius equal to $D_o/2$; $t = 0$, $P_C = P_B = P_{atm} + \rho_L g H_L + 4\sigma/D_o$) and the boundary conditions (the n point is fixed to the orifice perimeter, there are no interactions between bubbles, due to the low gas flow rate, the liquid is stagnant, $\alpha_L \simeq 1$) exposed in [22,24], two more considerations have to be pointed out.

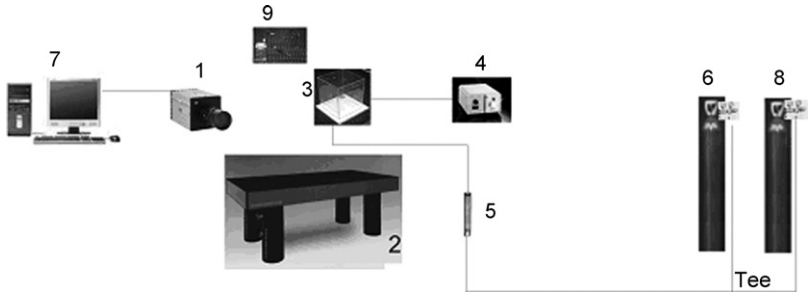

Fig. 3. Experimental setup: 1, high speed video camera; 2, optical table; 3, bubble column; 4, fiber optic; 5, rotameter; 6, compressed air; 7, computer; 8, compressed nitrogen; 9, oxygen electrode.

The first corresponds to:

$$(C_{O_2})_{liq} = 0.6C^*, \quad \text{at } t = 0 \tag{37}$$

Due to the experimental set up, shown in Fig. 3, the liquid in the bubble column was easily deoxygenated until the oxygen concentration was 60% of the saturation concentration at 20 °C. The videos were recorded then. As the detachment time is small, the oxygen concentration of the liquid at which the experimental bubble grows can be considered constant and equal to $0.6C^*$. The simulated bubble must grow under this concentration of oxygen in the liquid phase.

The second consideration has already been explained. It corresponds to the initial mass of the bubble once the bubble has detached, calculated from the mass inside the volume given by Eq. (32) from point 1 to the point in which the neck collapses, just at the detachment of the bubble

$$m_{t=\text{detachment}} = V_B \rho_G \tag{38}$$

The solution procedure can be summarised as follows. Both, the momentum (Eq. (8)) and the force balance (Eq. (13)), together with the calculation of the pressure drop across the orifice (Eq. (28)) and the mass balance to the gas chamber in terms of pressure (Eq. (29)) conform a system of coupled ODEs. The equations are implemented and solved using a combination of routines written in Matlab®. As a result, the bubble surface is calculated coupling the effects of expansion and rising for the r and z axis, providing dR/dt and dz'/dt. dR/dt is the velocity of the radial expansion of the bubble and dz'/dt is the only component (vertical) of the bubble rising while still attached to the orifice. Then, the global vertical and horizontal components of the velocity are determined using Eqs. (19) and (20). When the bubble has detached, Eq. (13) is substituted by Eq. (21), Eq. (29) becomes 0 and Eqs. (20) and (28) become Eqs. (22) and (34), respectively.

3. Materials and methods

3.1. Equipment

The experimental setup is shown in Fig. 3. The bubbles were recorded by means of a high speed video camera with recording speeds up to 1000 frames per second. The camera is held by a mechanic arm fixed on top of an optical table. Images are edited and analysed with the MOTIONSCOPE® software.

The air bubbles were generated in a bubble column with a square cross sectional area of 15 cm × 15 cm, made from flat glass walls of 20 cm of height to avoid distortions in the recording of the bubbles. The bubble column is placed on the optical table, justified with the camera. Glued to the bottom of the bubble column, there is a plastic cylinder to protect an air tube from the air bottle and to permit the generation of the bubbles at a certain height from the bottom of the tank, making easier the recording of the growing bubbles. Above the cylinder, a gas chamber of 8×10^{-6} m^3 is fixed. The gas chamber is directly fed from a gas bottle. At the top of the gas chamber, the stainless steal sieve plates are glued. The liquid height above the sieve plates is 8 cm.

Bubbles are generated from 1.5 mm and 2 mm diameter submerged orifices bore at the sieve plates using gas flow rates of $Q_C = 1$, 5 and 10×10^{-6} m^3 s^{-1}. The gas flow rates were measured by a rotameter located between the gas bottle and the bubble column. Two different liquids (water and carboxymethyl cellulose, CMC, Sigma C-5678 solution of 1.4%) at 20 °C are used to simulate the aeration in sieve plate tower reactors. The gas flow rates and the dimensions of the tank, made it possible to consider the liquid inside as stagnant.

In order to accurately simulate the mass transfer during the bubble formation process, every liquid was deoxygenated with a nitrogen flow until the oxygen concentration in the liquid is 60% of the saturation concentration, measured by an oxygen electrode Crison 92, for economical and experimental reasons. Since bubble generation require a short time, it is possible to experimentally fix the oxygen concentration in the liquid to $0.6C^*$, to compare the theoretical and the experimental bubble shapes.

3.2. Fluid properties

For the air–water system D_L is 2.1×10^{-9} m^2 s^{-1} [32], while for the CMC solution $0.69D_{L(\text{water–air})}$ [35]. The other important physical properties used in the model are:

water (20 °C, $\rho_L = 998$ kg m^3, $\sigma = 0.073$ N/m,

$\mu_L = 1.037 \times 10^{-3}$ Pa s).

The rheology of the CMC solution is determined using a rotational viscosimeter (Visco elite – L, Fungilab S.A.).

1.4% CMC in water (20 °C, $\rho_L = 1003$ kg m^3, $\sigma = 0.067$ N/m,

power law behaviour $m_f = 0.502$, $n = 0.750$).

4. Results and discussion

The comparison between experimental and theoretical shapes is straightforward as well as the detachment times. The volumes and the surface areas were also measured. One example for each rheological behaviour is shown.

4.1. Bubbles generated in Newtonian fluids

The volumetric mass transfer coefficient, $k_L a$, is composed of two terms. k_L depends on the microscopic movement of the molecules. a is the surface area whose profile is graphically determined during the bubble growth. When k_L is combined with a, the result shows a big increment during the formation stage of the bubble. The profile of "k_L" and "a" during the formation of a growing bubble, $D_o = 2$ mm, $Q_C = 5 \times 10^{-6}$ m^3 s^{-1}, is shown in Fig. 4. Experimental and simulated bubble areas are similar.

The comparison between bubble simulated shapes and bubble photographs for the same experiment can be seen in Fig. 5. Good agreement is achieved. The differences found between the photographs and the simulated shapes are focused on the lower part of the bubbles. The discretization of the bubbles in 100 points from the start of the growing process, avoided the inclusion of fictitious interpolated points during the expansion and rising of the bubble, a typical technique used by other authors [36]. However, only a few points were responsible for the development of the neck which determines the shape of the bubble in its lower region.

The results of this study and those presented in case of absence of mass transfer [24] are very similar, within the experimental recording error ±1 ms (Table 1). The effect of the mass transfer on the detachment time cannot be experimentally proved.

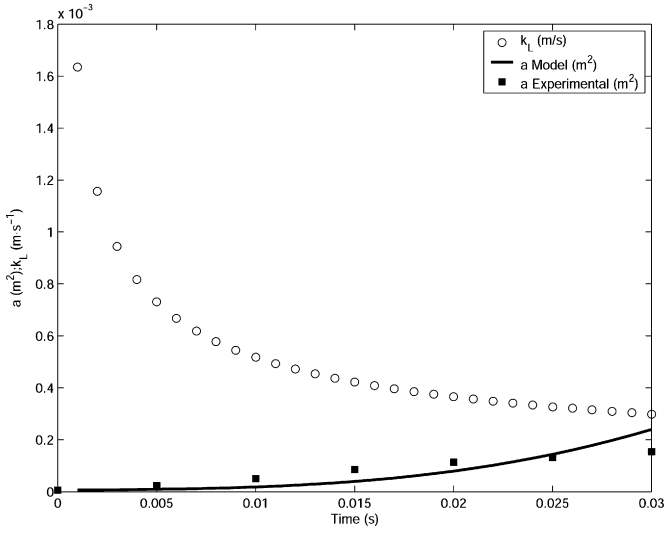

Fig. 4. k_L and a profiles while bubble growth in an inviscid fluid.

Fig. 6 shows the resistances to the mass transfer in the case of the air–water system. The most important resistance is that of the liquid phase. The three resistances increase with the formation time of the bubble.

4.2. Bubbles generated in non-Newtonian fluids

The present model accurately predicts several characteristics of the bubbles generated in non-Newtonian fluids like the formation time, the bubble volume, shape and surface area, under mass transfer conditions.

Fig. 7 represents the profile of both, "k_L" and "a". Experimental and calculated areas are plotted. The results are similar. Table 2 represents the recorded and the calculated detachment time of the bubbles under different experimental conditions.

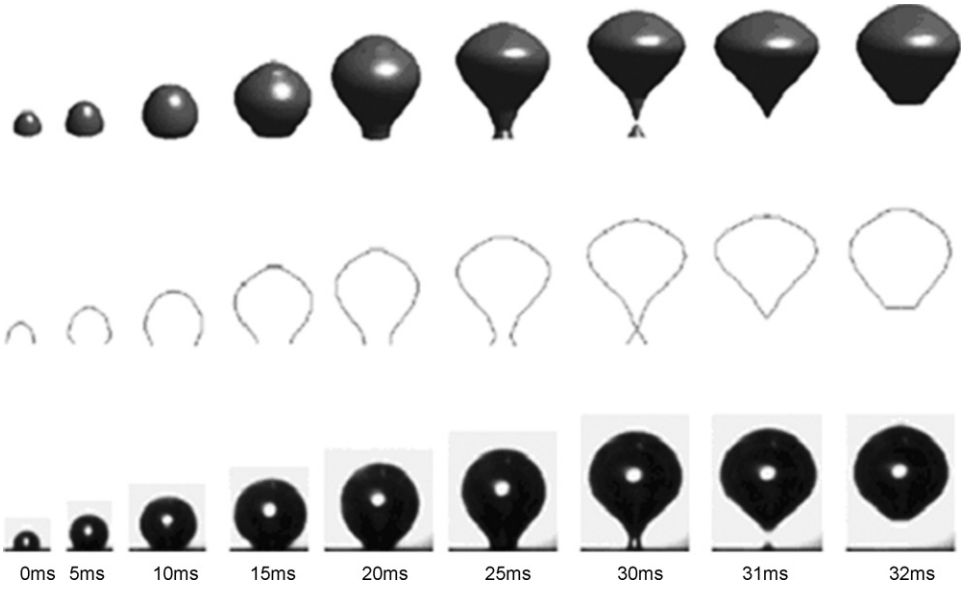

Fig. 5. Theoretical–experimental comparison $D_o = 2$ mm; $Q_C = 5 \times 10^{-6}$ m^3 s^{-1}.

Table 1
Time formation comparison

D_o (mm)	Q_C ($\times 10^6$ m^3 s^{-1})	Detach time (ms) (±1 ms experimental)	Detach time (ms) (±0.05 ms)
1.5	1	20	21
	5	20	19
	10	18	17
2	1	32	30
	5	30	30
	10	30	30

Higbie's theory; in Newtonian inviscid fluids.

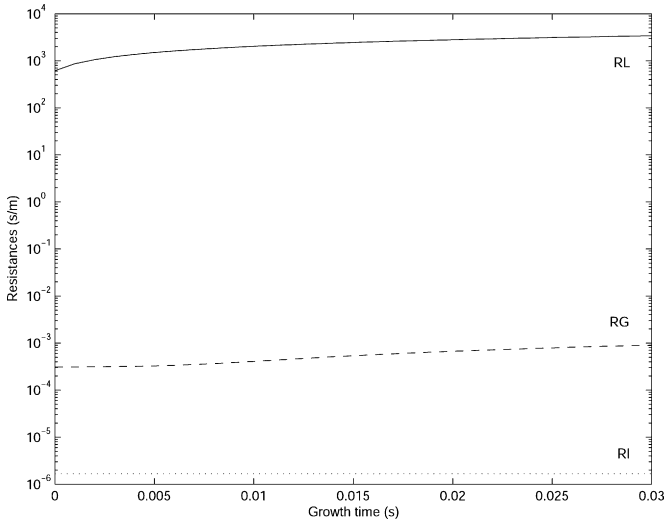

Fig. 6. Mass transfer resistances in water, $D_o = 2$ mm; $Q_C = 5 \times 10^{-6}$ m^3 s^{-1}.

Table 2
Time formation comparison

D_o (mm)	Q_C ($\times 10^6$ m^3 s^{-1})	Detach time (ms) (±1 ms experimental)	Detach time (ms) (±0.05 ms)
1.5	1	32	29
	5	31	28
	10	31	30
2	1	37	36
	5	36	36
	10	36	35

Higbie's theory; in non-Newtonian viscous fluid.

Reasonable good agreement has been found between them. The theoretical shapes are also in good agreement with the experimental pictures, Fig. 8. In this case, the bubbles are more spherical than when they were generated in inviscid fluids like water. The viscosity of the liquid medium, since both have similar surface tension, reduces the deformability of the bubble, its expansion, and slows down the growing, allowing a better fit between the experimental and the calculated shapes.

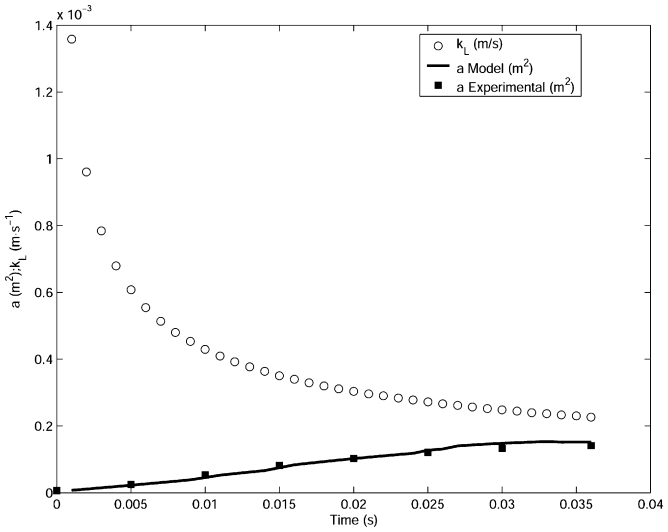

Fig. 7. k_L and a profiles profile while bubble growth in a viscous fluid.

As in the Newtonian case above mentioned, the model predicts a bubble formation times within the recording error than those presented previously in absence of mass transfer [24].

For a fixed flow rate, the experimental and the calculated values of the volume profile with time are found to be in good agreement up to the detachment time for both, water and the 1.4% CMC solution in water. Fig. 9 shows an example of the volume profile either simulated or experimental, calculated from the photographed bubbles. Constant flow regime is shown, bubble volume is proportional to the detachment time, and good agreement was found between the experimental and the simulated values.

The mass transfer mechanism in case of the non-Newtonian rheological behaviour is shown in Fig. 10 for $Q_C = 5 \times 10^{-6}$ m^3 s^{-1} and $D_o = 2$ mm. The most important resistance to the oxygen transfer is that of the liquid phase and is nearly constant during the major part of the formation process. The liquid resistance to the mass transfer directly depends on the diffusivity. So, the reduction of the diffusivity when increasing the viscosity of the liquid phase will decrease the k_L. On the other hand, the increment in the formation time, due to the increase in the viscosity of the liquid, also results in a longer time with a higher mass transfer resistance to the transport with respect to

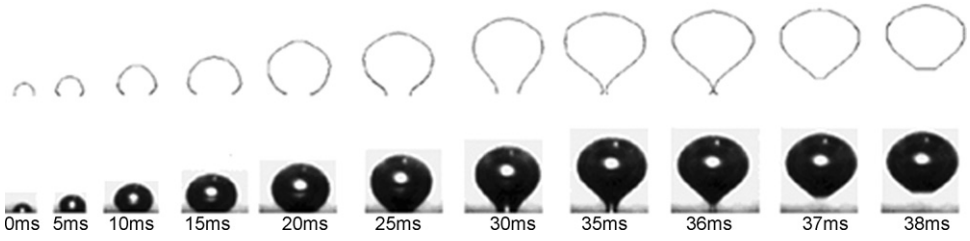

Fig. 8. Theoretical–experimental comparison $D_o = 2$ mm; $Q_C = 5 \times 10^{-6}$ m^3 s^{-1}.

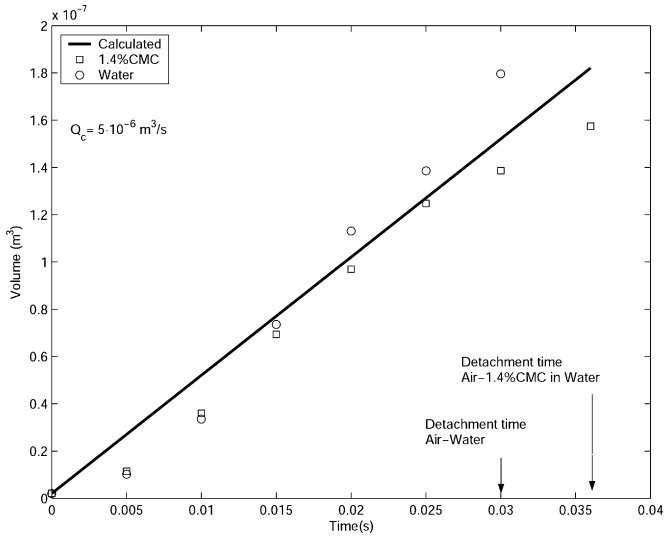

Fig. 9. Theoretical–experimental comparison for the volume profile in inviscid and viscous fluids $D_o = 2$ mm; $Q_C = 5 \times 10^{-6}$ m^3 s^{-1}.

the obtained for the air–water system. The combination of the two effects results in a decrease in the volumetric mass transfer coefficient with the increment in the viscosity.

4.3. Theoretical effect of the physical properties of the liquid on the mass transfer

Using the verified model, it is possible to study the isolated effect of the physical properties of the liquid on the mass transfer from a single growing bubble in a Newtonian medium. The working ranges of the liquid viscosity, liquid density and surface tension used in the simulations are summarised in Table 3. In the simulations, the properties are changed one at a time. The concentration of oxygen in the liquid is considered to be 60% of the saturation concentration, as has been used so far.

The wide range of liquid fluids operating in a bubble column and the change in their properties during some of the processes

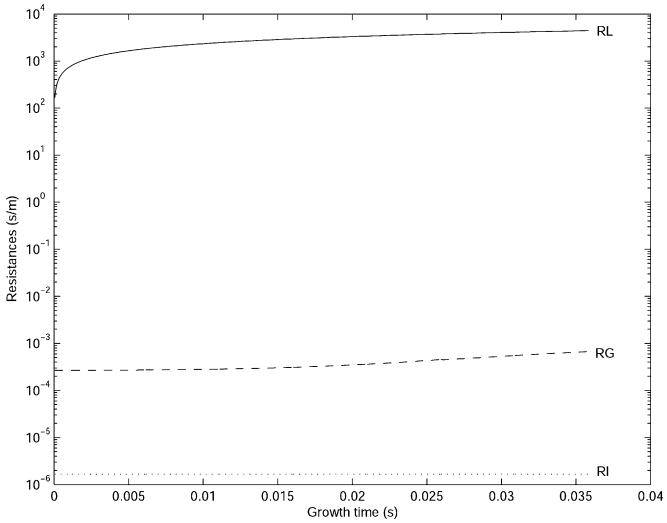

Fig. 10. Mass transfer resistances in viscous fluid, $D_o = 2$ mm; $Q_C = 5 \times 10^{-6}$ m^3 s^{-1}.

Table 3
Values of the different liquid properties and gas flow rates used during the theoretical simulations using a Newtonian fluid

D_o (mm)	Q_C (cm^3 s^{-1})	ρ (kg m^{-3})	σ (mN m^{-1})	μ (mPa s)
1.5	1	750	18.2	1
		900	36.5	5
		998	54.7	10
		1125	73.0	25
		1250	91.2	50
			109.5	100
1.5	5	750	18.2	1
		998	36.5	5
		1250	73.0	10
			109.5	25
				50
				100
2.0	1	750	18.2	1
	5	998	36.5	5
		1250	73.0	10
			109.5	25
				50
				100

taking place inside [4,19–21] spread the spectrum of the viscosities of the liquid phase. The liquid viscosity has two effects on the hydrodynamics of the bubble. First, it slows down the bubble expansion, and second, it slows down the molecular movement at the surface of the bubble, which delays the generation of the bubble neck and the detachment of the bubble. At the same time, the retardation of the molecular movement reduces the diffusivity. The change in the viscosity of the liquid medium during the process, can even shift the rheological behaviour of the liquid from Newtonian to non-Newtonian.

The effect of the liquid viscosity on the liquid diffusivity can be calculated by Eq. (38), proposed by Öztürk et al. [23]:

$$D_L = 5.0 \times 10^{-11} \mu_L^{-0.57} \quad (38)$$

The increment in the liquid resistance and its profile with time for liquid viscosities from that of water at 20 °C to 100 times bigger, is shown in Fig. 11. The increment in the viscosity of the liquid, similar to the one which takes place during a fermentation process for example, reduces the molecular transport. However, the surface area of the bubble increases, because there is an increment in the formation time of the bubble. If a gas flow rate is to be maintained, the generation of bigger bubbles results in a little number of them, and in this case the specific area also decreases with the viscosity. Therefore, the volumetric mass transfer coefficient decreases with the viscosity.

The variation of the Sherwood number with time is calculated using the definition of the Sherwood number. The characteristic length is defined as the equivalent diameter for the sphere with the same volume as that of the bubble at a given time. Fig. 12 shows a reduction in the Sherwood number during the generation of the bubble. The decrease of diffusivity affects more powerfully on the Sherwood number than the increase in the equivalent diameter.

Apart from the different liquids used in a bubble column, the generation of alcohols, acids, etc. during a fermentation process,

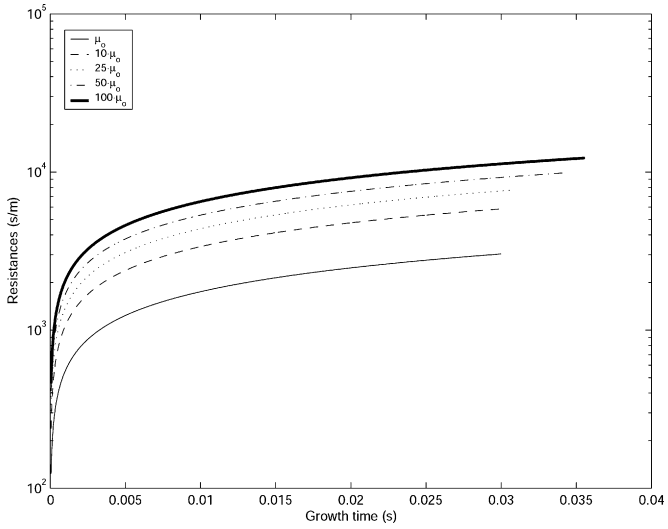

Fig. 11. Liquid resistance profile with time. Effect of the liquid viscosity.

modifies the surface tension during the process [20,21,36–38]. This fact will affect the detachment time of the bubbles, since the surface tension determines the expansion of the bubble and the break up or the collapse of its neck. Once detached, during the rising movement of the bubbles, the variation of the surface tension will modify the oscillatory behaviour, determining he concentration profile surrounding the bubbles. It has been proved than the oscillations enhance the mass transfer rates from the bubbles [15,39]. So far, the conclusions have not resulted in a consensus agreement about the effect of the surface tension on the oxygen transfer rate [19,40–43], but it has been proved that lowering the surface tension in an aerated media result in an increase in the growth of anaerobic bacteria at the interface [44].

Besides the liquid viscosity and the surface tension, the density of the different liquids also shows a wide range. The liquid density determines the buoyancy of the bubbles and constitutes

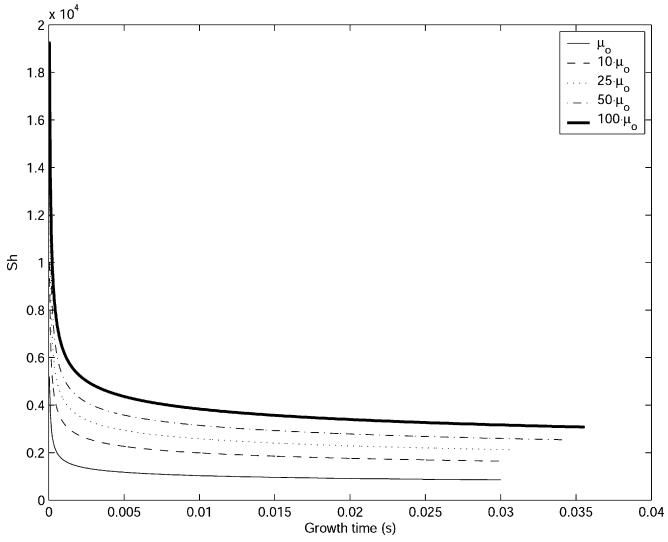

Fig. 12. Sherwood profile during the formation of a bubble. Effect of the viscosity of the liquid.

a resistance for their expansion in the liquid phase, determining the bubble initial volume.

As can be seen in Fig. 12, the Sherwood number soon reaches an almost constant value. The values of the Sherwood number at the detachment time of the bubble can be considered representative for the bubble formation. The effect of the physical properties of the liquid on the Sherwood number of a growing bubble can be studied, using the same definition of the characteristic length as that mentioned before for Fig. 12, and the formation time of the bubbles as function of the physical properties of the liquid obtained by the modified model proposed in the present paper, along with the predictive equation for the diffusivity, Eq. (38).

Fig. 13 represents the results for bubbles generated from a sieve plate with a hole of $D_o = 2$ mm and $Q_C = 5 \times 10^{-6}$ m^3 s^{-1}. Liquid viscosity and surface tension increase the Sherwood number, meanwhile the effect of the density is small.

In order to rationalize and give an insight of the effect of the typical physical properties of the liquid, viscosity, surface tension and density, on the Sherwood number for a growing bubble, a dimensionless study has been carried out using the Reynolds, the Grashof and the Schmidt dimensionless numbers.

An equation for the Sherwood number similar to those proposed by other authors [26] can be obtained:

$$Sh = 10Re^{0.24}Sc^{0.32} \tag{39}$$

The exponents of the dimensionless numbers in Eq. (39) correspond to the predictions of [45], because the exponent of the *Sc* is similar to 1/3 and the exponent of the *Re* depends on the system, and is similar to 1/4. Using the Grashof number instead of the Reynolds number

$$Sh = 1.3Gr^{0.23}Sc^{0.45} \tag{40}$$

Better fit is achieved using Eq. (39). Fig. 14 represents the Sherwood number as function of the dimensionless numbers *Re* and *Sc*. The coefficients of the dimensionless numbers are in the same order than those proposed for the rising bubbles, bigger coefficient for the *Sc* number than for the *Re* or *Gr* numbers.

Due to the quick surface removal during the growing of the bubble, the Sherwood numbers are high. Besides the marked effect of the viscosity, increasing the Sherwood number as it decreases the molecular movement and, with it, the diffusion coefficient, the liquid density reduces the Sherwood number. Its effect is small, because the liquid density affects directly the buoyancy of the bubbles and reduces the expansion. Its effect is shown on the dimensionless numbers regarding the fluid flow, the Reynolds or the Grashof numbers, and the Schmidt number, which accounts for the molecular movement. The slowed down of the expansion, due to the increment in the liquid density, is more important than the increment in the buoyancy, leading to a reduction in the surface removal and so, in the Sherwood number. Furthermore, the surface tension also determines the bubble expansion, the bubble formation time and its equivalent diameter. An increase in the surface tension reduces the bubble volume. The bubbles tend to be more spherical and small to reduce the superficial energy [24]. The Sherwood number is directly related

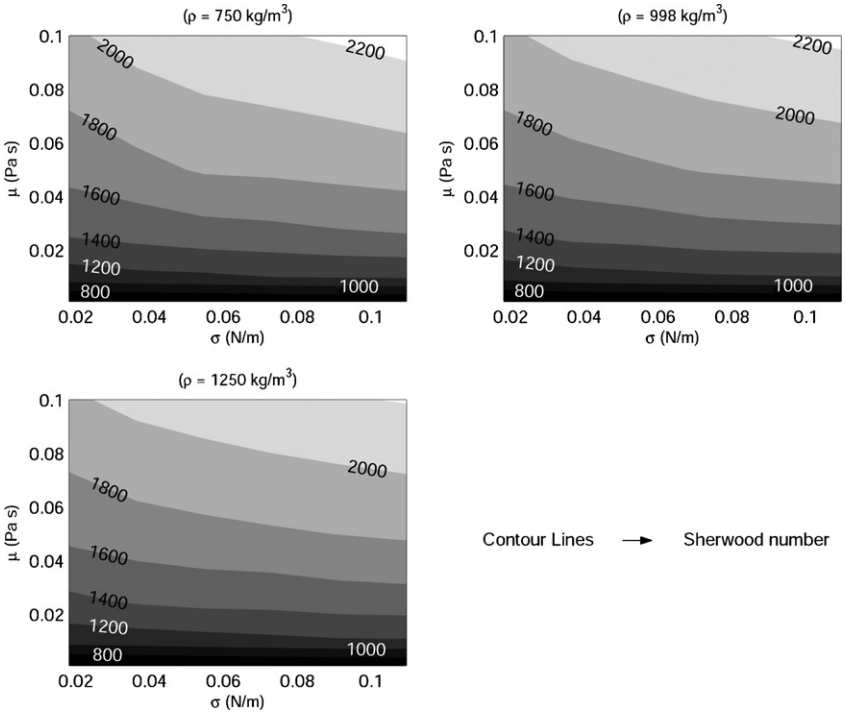

Fig. 13. Effect of the physical properties of the liquid on the Sherwood number. $D_o = 2$ mm. $Q_C = 5 \times 10^{-6}$ m^3 s^{-1}.

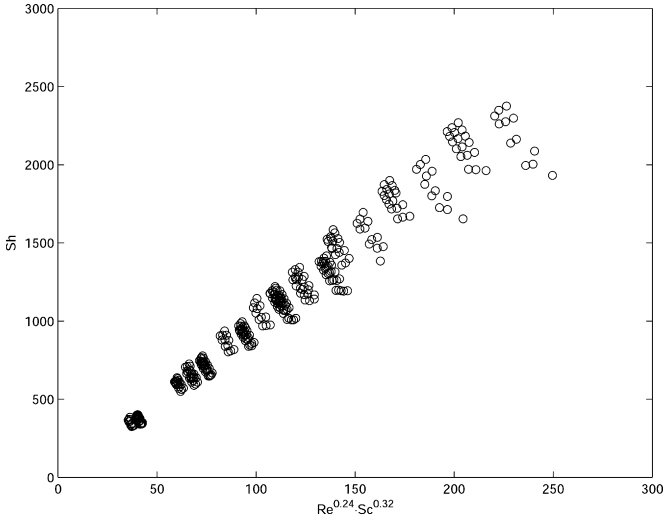

Fig. 14. Sherwood vs. Reynolds and Schmidt numbers, Eq. (39).

to the equivalent diameter but it is also determined by the liquid resistance, k_L, which depends on the formation time. The surface tension reduces the formation time [22]. From the combination of both influences, the Sherwood number reduces as the equivalent diameter increases, but this effect is small, and the surface tension increases the Sherwood number.

5. Conclusions

The mass transfer mechanism from single growing bubble in Newtonian and non-Newtonian media has been successfully studied by means of traditional concepts in the calculation of global mass transfer coefficients. This model predicts bubble shapes and initial conditions for bubble oscillations after detachment with a good agreement with the experimental recordings in deoxygenated liquids.

The gap between detachment time with or without mass transfer is small. When the liquid media was viscous, the stabilization of the bubble neck resulted in detachment times that almost copy those obtained for the systems in absence of mass transfer.

From the study of the effect of the physical properties of the liquid on the mass transfer several results can be obtained. The effect of the viscosity is marked because not only determines the bubble formation time, but also the diffusion coefficient, and it finally results in an increment in the Sherwood number and a decrease in the mass transfer resistance k_L. The liquid density, responsible for the buoyancy of the bubble and its expansion, reduces the Sherwood number, meanwhile the surface tension, which determines the bubble shape its and expansion, increases the Sherwood number. The calculated Sherwood number can be correlated as function of dimensionless numbers defining the flow, the movement of the bubble and the diffusional process like *Re*, *Gr* and *Sc* similarly to the correlations presented for rising bubbles [23–25] with good results.

Acknowledgments

The support of the Ministerio de Educación y Ciencia of Spain providing a F.P.U. fellowship to M. Martín is greatly welcomed. The funds from the project reference PPQ2000-0097-P4-02 are also appreciated.

References

[1] Y.T. Shah, B.G. Kelkar, S.P. Godbole, W.D. Deckwer, Design parameters estimations for bubble column reactors, AIChE J. 28 (3) (1982) 353–374.

[2] R. Krishna, A scale up strategy for a commercial scale bubble column slurry reactor Fischer–Tropsch synthesis, Oil Gas Sci. Technol. 55 (4) (2000) 359–393.

[3] R. Krishna, J.M. van Baten, Mass transfer in bubble columns, Catal. Today 79–80 (2003) 67–75.

[4] N. Kantarci, F. Borak, K.O. Ulgen, Review: bubble column reactor, Process Biochem. 40 (7) (2005) 2263–2283.

[5] P.R. Gogate, A.A.C.M. Beenackers, A.B. Pandit, Multiple-impeller systems with a special emphasis on bioreactors: a critical review, Biochem. Eng. J. 6 (2000) 109–144.

[6] H.C. Vogel, C.L. Todaro, Fermentation and Biochemical Engineering Handbook Principles, Process Design and Equipment, Noyes Publications, New Jersey, 1996.

[7] P.F. Davis, A. Remuzzi, E.J. Gordon, C.F. Dewey, M.A. Gimbrone Jr., Turbulent fluid shear stresses induces vascular endothelial cell turnover in vitro, Proc. Natl. Acad. Sci. U.S.A. 83 (1986) 2114–2117.

[8] J. Hua, L.E. Erickson, T.Y. Yiin, L.A. Glasgow, A review of the effects of shear and interfacial phenomena on cell viability, CRC Crit. Rev. Biotechnol. 13 (1993) 305–328.

[9] S.P. Godbole, A. Schupe, Y.T. Shah, N.L. Carr, Hydrodynamics and mass transfer in non-Newtonian solutions in a bubble column, AIChE J. 30 (2) (1984) 213–220.

[10] R. Higbie, The rate of absorption of a pure gas into a still liquid during a short time of exposure, Trans. Am. Inst. Chem. Eng. 31 (1935) 365–389.

[11] F. Takemura, A. Yabe, Gas dissolution process of spherical rising gas bubbles, Chem. Eng. Sci. 53 (15) (1998) 2691–2699.

[12] F. Takemura, Y. Matsumoto, Dissolution rate of spherical carbon dioxide bubbles in strong alkaline solutions, Chem. Eng. Sci. 55 (2000) 3907–3917.

[13] B. Zhao, J. Wang, W. Yang, Y. Jin, Gas–liquid mass transfer in slurry bubble systems. I. Mathematical modelling based on a single bubble mechanism, Chem. Eng. Sci. 96 (2003) 23–27.

[14] B. Haut, T. Cartageb, Mathematical modeling of gas–liquid mass transfer rate in bubble columns, Chem. Eng. Sci. 60 (22) (2005) 5937–5944.

[15] F.J. Montes, M.A. Galán, R.L. Cerro, Mass transfer from oscillating bubbles in bioreactors, Chem. Eng. Sci. 54 (1999) 3127–3136.

[16] P.H. Calderbank, R.P. Patra, Mass transfer in the liquid phase during the formation of bubbles, Chem. Eng. Sci. 21 (8) (1966) 719–721.

[17] K. Terasaka, J. Oka, H. Tsuge, Ammonia absorption from a bubble expanding at a submerged orifice into water, Chem. Eng. Sci. 57 (18) (2002) 3757–3765.

[18] K. Terasaka, H. Tsuge, Bubble formation at a single orifice in non-Newtonian liquids, Chem. Eng. Sci 46 (1) (1991) 85–93.

[19] F.H. Deindoerfer, J.L. Gaden Jr., Effects of liquid physical properties on oxygen transfer in penicillin fermentation, Appl. Environ. Microbiol. 3 (1955) 253–257.

[20] M. Rudis, V. Jezdinsky, Z. Sterbacek, Physical properties of microbial suspensions. II. Properties of microbial suspensions and their supernatants during fermentation conditions, Folia Microbiol. (Praha) 22 (2) (1977) 128–133.

[21] R.W. Silman, Continuous estimation of viscosity, fluid density, surface tension, and heat output during fermentations, Biotechnol. Tech. 2 (4) (1988) 221–226.

[22] M. Martín, F.J. Montes, M.A. Galán, On the influence of liquid physical properties on bubble volume and generation times, Chem. Eng. Sci. 61 (2006) 5196–5203.

[23] S.S. Öztürk, A. Schumpe, W.D. Deckwer, Organic liquids in a bubble column: Holdups and mass transfer coefficients, AIChE J. 33 (9) (1987) 1473–1480.

[24] M. Martín, F.J. Montes, M.A. Galán, Numerical calculation of shapes and detachment times of bubbles generated from a sieve plate, Chem. Eng. Sci. 61 (2006) 363–369.

[25] N. Frössling, Uber die verdunstung fallenden tropfen (evaporation of falling drops), Gerlands Beitage Geophys. 52 (1938) 170–216 [English ranslation: Griffith (1960) Mass transfer from drops and bubbles, Chem. Eng. Sci., 12, 198–213].

[26] P.H. Calderbank, M.B. Moo-Young, The continuous phase heat and mass transfer properties of dispersions, Chem. Eng. Sci. 16 (1961) 39–54.

[27] G.A. Hughmark, Hold-up and mass transfer in bubble columns, Ind. Eng. Chem. Proc. Des. Dev. 6 (2) (1967) 218–220.

[28] H.Z. Li, Y. Mouline, N. Midoux, Modelling the bubble formation dynamics in non-Newtonian fluids, Chem. Eng. Sci. 57 (2002) 339–346.

[29] K. Loubière, G. Hébrard, Bubble formation from a flexible hole submerged in an inviscid liquid, Chem. Eng. Sci. 58 (1) (2003) 135–148.

[30] V.C. Kelessidis, Terminal velocity of solid spheres falling in Newtonian and non-Newtonian liquids, Tech. Chron. Sci. 1–2 (2003) 43–54.

[31] T.K. Sherwood, R.L. Pigford, C.R. Wilke, Mass Transfer, McGraw Hill, New York, 1975.

[32] G. Grund, A. Schumpe, W.D. Decwer, Gas–liquid mass transfer in a bubble column with organic liquids, Chem. Eng. Sci. 47 (13/14) (1992) 3509–3516.

[33] R.W. Fox, A.T. McDonald, Introduction to Fluid Mechanics, 4th ed., McGraw Hill, New Cork, 1995.

[34] B. Demidovich, Problemas y ejercicios de análisis matemático, 11th ed., Paraninfo, Madrid, 1993, pp. 171, 176.

[35] K.K. Tan, R.B. Thorpe, Gas diffusion into viscous and non-Newtonian liquids, Chem. Eng. Sci. 47 (13/14) (1992) 3565–3572.

[36] H.N. Oguz, A. Prosperetti, Dynamics of bubble growth and detachment from a needle, J. Fluid Mech. 257 (1993) 111–144.

[37] C.L. Queiroga, R.L. Nascimento, G.L. Serra, Evaluation of paraffins biodegradation and biosurfactant production by bacillus subtilis in the presence of crude oil, Br. J. Micorbiol. 34 (2003) 321–324.

[38] H. Rashedi, E. Jamshidi, M. Mazaheri Assadi, B. Bonakdarpour, Isolation and production of biosurfactant from Pseudomonas aeruginosa isolated from Iranian southern wells oil, Int. J. Environ. Sci. Technol. 2 (2) (2005) 121–127.

[39] M. Martín, F.J. Montes, M.A. Galán, Prediction of the volumetric mass transfer coefficient: the case of the oscillating bubble, Chem. Eng. Sci., submitted for publication.

[40] A.I. Downing, G.A. Trusdale, Some factors affecting the rate of solution of oxygen in water, J. Appl. Chem. 5 (10) (1955) 570–581.

[41] A.I. Downing, K.V. Melbourn, A.M. Bruce, The effect of contaminants on the rate of aeration of water, J. Appl. Chem. 7 (11) (1957) 590–596.

[42] R. Manganelli, Detergents and sewage treatment, Sewage Works 24 (9) (1957) 1057–1068.

[43] H.J. Hwang, M.K. Stenstrom, The effect of surface active agents on oxygen transfer, 1979. Technical Report, Water Resources Program, School of Engineering and Applied Science, University of California, Los Angeles, Los Angeles, California.

[44] Larson, Cantwell, Hartzell, J. Infect. Dis. 25 (1919) 41.

[45] J.T. Davies, Turbulence Phenomena, Academia Press, New York, 1972.